Distortions to the penetration depth and coherence length of superconductor/normal-metal superlattices

P. Quarterman, Nathan Satchell, Satc

Abstract

Superconducting (S) thin film superlattices composed of Nb and a normal metal spacer (N) have been extensively utilized in Josephson junctions given their favorable surface roughness compared to Nb thin films of comparable thickness. In this work, we characterize the London penetration depth and Ginzburg-Landau coherence length of S/N superlattices using polarized neutron reflectometry and electrical transport. Despite the normal metal spacer layer being significantly thinner than the coherence length, we find that the introduction of a thin N spacer between S layers leads to a dramatic increase in the London penetration depth and a decrease in the coherence length. Furthermore, the temperature dependence of the upper critical field suggests that the superlattices act as a layered 2D superconductor, despite the N thickness being more than a factor of two smaller than when such a 2D state is expected to occur. Using the measured values for the penetration depth and coherence length, we experimentally determine the Ginzburg-Landau parameter to quantify the superconducting disorder of the superlattice samples and compare to a single Nb thin film sample.

^{*} patrick.quarterman@nist.gov

[†] N.D.Satchell@leeds.ac.uk

I. INTRODUCTION

Superconducting materials have long been of interest since they were first discovered in 1911 by Kammerlingh Onnes [1]. The two fundamental properties most closely associated with superconductivity are zero electrical resistance and the expulsion of magnetic field, where the latter is known as the Meissner effect [2]. The two typical lengthscales describing superconductivity are the coherence length (ξ) and the penetration depth (λ), which we set out to measure directly in this work. The ratio of these two length scales, known as the Ginzburg-Landau parameter ($\kappa = \lambda/\xi$), governs whether the superconductor is type-I or type-II, where a type-I is defined as $\kappa < 1/\sqrt{2}$ and type-II when $\kappa > 1/\sqrt{2}$. In bulk single crystal, Nb is a borderline type-I/type-II superconductor with $\xi \approx \lambda \approx 41$ nm [3]. Upon reducing dimensionality and introducing the disorder associated with polycrystalline thin film growth, Nb becomes strongly type-II with a typical κ between 8 and 10.

Superconducting technologies based on Josephson junctions are a promising candidate for a low power computational alternative to traditional CMOS technologies [4, 5]. Of particular interest, here, are ferromagnetic Josephson junctions which form the memory bits in such a scheme [6–18]. There have been numerous reports concerning the supercurrent passing through ferromagnetic Josephson junctions, including the discovery of spin triplet pair correlations in these systems [19–26]. In order to improve the properties of the thin ferromagnetic layers in the Josephson junctions, it is important that the surface roughness of the Nb electrode be as small as possible [27]. It has long been known that introducing a thin Al layer between Nb films improves the surface roughness compared to Nb films of equivalent thickness; this is understood to be due to the Al forming amorphously and thus preventing columnar growth of Nb [28–30]. Given that the Al is sufficiently thin in these multilayers, the Al layer superconducts via proximity effect from the neighboring Nb layers. It has previously been shown that by replacing Nb with a Nb/Al superlattice, the curious effect of non-linear scaling of critical currents with area can be resolved [31]. Recently, it was discovered that replacing Al with Au has the same effect on the surface roughness of the superlattice, as we report in this work.

The London penetration depth ($\lambda_{\rm L}$) characterizes the depth of penetration of an externally applied field and is the length scale associated to the Meissner effect, hence it is often referred to as the magnetic screening length [3]. $\lambda_{\rm L}$ is typically determined from measure-

ments of flux expulsion by muon implantation [32] or surface microwave [33] techniques.

In superconducting thin film samples, when an in situ magnetic field is applied and the samples are cooled below the superconducting transition temperature, polarized neutron reflectometry (PNR) is sensitive to the absence of magnetic field due to the Meissner effect as a function of depth [34–36]. The availability of PNR makes this technique highly attractive for the study of thin films with buried interfaces. PNR directly probes the nuclear composition and magnetization, as a function of depth, in thin film systems. The non-spin flip reflectivities $(R^{\uparrow\uparrow})$ and $R^{\downarrow\downarrow}$ are sensitive to the nuclear composition and in-plane magnetization, aligned with the in situ magnetic field, as a function of depth through the sample. Han et al examined Nb/Al superlattices near and above the lower critical field by measuring the penetration depth (λ_L) and characterizing the formation of superconducting vortices using PNR [37]. After the early investigations of field expulsion in superconducting thin film systems, PNR characterization of superconductors became less common due to the unavailability of sufficiently smooth interfaces in thin film materials with novel properties. Early attempts to study thin films of YBCO, for example, had limited success due to the large surface roughness [35]. Recently, improvements in thin film growth combined with experimental observations and theoretical predictions of proximity effects in superconductor-ferromagnet (S/F) based heterostructures have renewed interest for characterizing the field expulsion profile in detail [38–44]. The PNR measurements and analysis performed here are expandable to a wide range of conventional and unconventional superconducting systems, and layered heterostructures containing both superconducting and non-superconducting layers. However, we wish to note that these measurements remain challenging due to the magnetic scattering length density due to expelled field of a superconductor being as much as two orders of magnitude lower than that of strong ferromagnets, such as Fe.

The Ginzburg-Landau coherence length ($\xi_{\rm GL}$) characterizes the distance over which superconductivity can vary without undue energy increase [45]. Experimentally, one can estimate $\xi_{\rm GL}$ from temperature-dependent electrical transport measurements of the upper critical field H_{c2} . In conventional bulk superconductors, H_{c2} is isotropic. In thin film and layered superconductors, the upper critical field for field orientations parallel ($H_{c2\parallel}$) and perpendicular ($H_{c2\perp}$) to the sample plane can differ significantly. To determine an accurate estimate for $\xi_{\rm GL}$, H_{c2} data must be analyzed in the appropriate geometric limit [45].

In this work, we directly determine the effects of introducing a thin (with respect to $\xi_{\rm GL}$)

non-superconducting layer (N, which is Al or Au) in Nb-dominant superlattices. Quantitative understanding of $\lambda_{\rm L}$ and $\xi_{\rm GL}$ are important for modelling and interpreting the behavior of superconducting devices such as Josephson junctions and Superconducting QUantum Interference Devices (SQUIDs), in which the use of superlattices to reduce surface roughness may be advantageous. For example, in a Josephson junction the characteristic Fraunhofer pattern is determined by the flux (Φ) in the junction, $\Phi = \mu_0 H w(2\lambda_L + d)$, where w is the width of the patterned junction and d is the thickness of the junction. However, this description is modified if $\lambda_{\rm L}$ becomes comparable to or longer than the thickness of the superconducting electrode, which is common in thin films [46]. As such, an independent and direct measurement of the $\lambda_{\rm L}$ is important for thorough characterization and understanding of these Josephson junctions. We find distinctly different superconducting properties of S/N superlattice samples compared to a single Nb thin film using PNR and electrical transport measurements. We observe large, consistent modification of $\lambda_{\rm L}$ and $\xi_{\rm GL}$, which allows us to directly probe and quantify the weakening of the superconducting coupling in the out-of-plane direction associated with the introduction of a thin normal metal intermediary layer.

We also report that while our Nb film is best described as a 3D superconductor, the superlattices are best described by the 2D limit of layered superconductors. Such 2D states have been observed in a number of different S/N superlattices, but as far as we know not in the composition of the two superlattices studied here [47]. When a superlattice is made by layering a superconductor with normal metals [48, 49], semiconductors [50, 51], or ferromagnets [52], measurements of H_{c2} (T) have long been known to show a transition from 3D to 2D superconductor behaviour when the temperature is reduced [47]. This crossover is understood to occur due to reduction of the perpendicular coherence length (ξ_{\perp}) to values shorter than the non-superconductor layer thickness, which results in a decoupling of the layers in the superlattice. Finally, given that our N layer is more than a factor of two smaller than $\xi_{GL\perp}$ at 0 K, our finding of a 2D $\xi_{GL\perp}$ ($H_{c2\parallel}$ (T)) is quite surprising.

II. EXPERIMENTAL METHODS

Thin films are deposited by sputtering with base pressure of 2×10^{-8} Torr and partial water pressure of 3×10^{-9} Torr $(4 \times 10^{-7} \text{ Pa})$, after liquid nitrogen cooling. We grow the films

on Si substrates, which have a native oxide layer. Growth is performed at an approximate Ar (6N purity) pressure of 2 mTorr and temperature of -25 °C. Triode sputtering is used for Nb and Al from 57 mm diameter targets, and dc magnetron sputtering is used for Au from a 24 mm diameter target. Materials are deposited at typical growth rates of 0.4 nm s⁻¹ for Nb and Au, and 0.2 nm s⁻¹ for Al from targets with 4N purity. Growth rates are calibrated using an *in situ* quartz crystal film thickness monitor and checked by fitting to Kiessig fringes obtained from X-ray reflectometry (XRR) on reference samples.

The superlattices had a full stack structure of $[S(25)/N(2.4)]_7/S(25)$, where the nominal thicknesses are denoted in nanometers, S refers to superconducting Nb, and N refers to Al or Au. Hereafter, the superlattice samples are referred to as Nb/Al or Nb/Au. The thicknesses of the S and N layers are guided by previous work [31], and the number of repeats chosen so the films were thick enough to give appreciable magnetic field screening to observe with PNR. In addition, a 200 nm film of Nb was grown for comparison to the superlattices in our current investigation and is comparable to Nb films described in previous studies [34, 35].

We collect PNR using the Polarized Beam Reflectometer and Multi-Angle Grazing-Incidence K-vector reflectometer at the NIST Center for Neutron Research (NCNR). The incident neutron spins are polarized parallel or antiparallel to the applied in-plane magnetic field (H) with supermirrors, and reflectivity is measured in the non-spin-flip cross sections $(R^{\uparrow\uparrow} \text{ and } R^{\downarrow\downarrow})$ as a function of the momentum transfer (Q) normal to the film surface. The PNR data are reduced and modeled using the REDUCTUS [53] software package and model-fit using the REFL1D program [54, 55]. The uncertainty of each fitting parameter is estimated using a Markov-chain Monte-Carlo simulation implemented by the DREAM algorithm in the BUMPS Python package, and with the number of steps taken allowing for the uncertainty to be reported with two significant digits [56]. Data are gathered at temperatures as low as 3 K, using a closed cycle refrigerator, and with an in situ magnetic field of 42 mT applied in the sample plane. To avoid concerns of flux trapping, we do not change field when below the transition temperature of Nb (≈ 9 K). When changing field states, the temperature is increased to approximately 12 K. For reproducibility of the magnetic field condition, a saturating field of 700 mT is then applied, followed by lowering to the desired measurement field, and finally the sample is cooled to the base temperature of 3 K. XRR and rocking curves are used to confirm the structural model determined from PNR. (An in-depth discussion of the XRR results can be found in the supplemental materials [57]).

Electrical transport measurements are performed using a conventional four-point-probe measurement configuration with lock-in amplifier and 100 μ A current source. We collect transport data in a ⁴He cryostat with variable temperature insert (1.3 - 300 K) and 8 T superconducting solenoid. Our resistance measurements are performed at a fixed temperature by continuously ramping the magnetic field. Resistance as a function of the in- and out-of-plane field, at various temperatures, determines the upper critical fields $(H_{c2\parallel}, H_{c2\perp})$. The Ginzburg-Landau coherence lengths in the plane and perpendicular to the plane are extracted by fitting to measurements of H_{c2} as a function of temperature [45].

III. RESULTS

The non-spin flip PNR and the spin asymmetry $[SA = (R^{\uparrow\uparrow} - R^{\downarrow\downarrow})/(R^{\uparrow\uparrow} + R^{\downarrow\downarrow})]$ for the Nb, Nb/Al and Nb/Au samples, measured at 42 mT, are shown in Fig. 1, alongside theoretical fits. The PNR Bragg peak spacing $(\Delta Q = 2\pi/t)$ shows that the superlattice structures are close to the nominal layer thicknesses, and the spin asymmetry serves to highlight the differences in scattering intensity between $R^{\uparrow\uparrow}$ and $R^{\downarrow\downarrow}$ induced by Meissner screening. For data taken at 20 K for the Nb/Al sample, we observe no observable spin asymmetry, as expected (supplemental Fig. 3 [57]). Specular and off-specular background XRR are collected in order to further validate the neutron reflectometry results as shown in supplementary Fig. 1 [57]. We also collect x-ray rocking curves to provide additional qualitative information about sample roughness, and the data can be seen in supplementary Fig. 2 [57].

The scattering length density (SLD) profiles that yield the best theoretical fits for the $R^{\uparrow\uparrow}$ and $R^{\downarrow\downarrow}$ data in Figs. 1 (a), (c), and (e) are shown in Fig. 2. When fitting the superlattice structure, each elemental layer is constrained to the same nuclear SLD and thickness. The nuclear scattering length densities are in strong agreement with the bulk values for each layer. We model the magnetic field expulsion as a function of depth (where z is distance from edge of the superconductor) in the superlattice using the London equation for a type-II superconductor [45],

$$B(z) = B_0 \cosh\left(\frac{z}{\lambda_{\rm L}} - \frac{d_s}{2\lambda_{\rm L}}\right) \cosh\left(\frac{d_s}{2\lambda_{\rm L}}\right)^{-1},\tag{1}$$

where d_s and z are the thickness of the superconductor and distance from the surface,

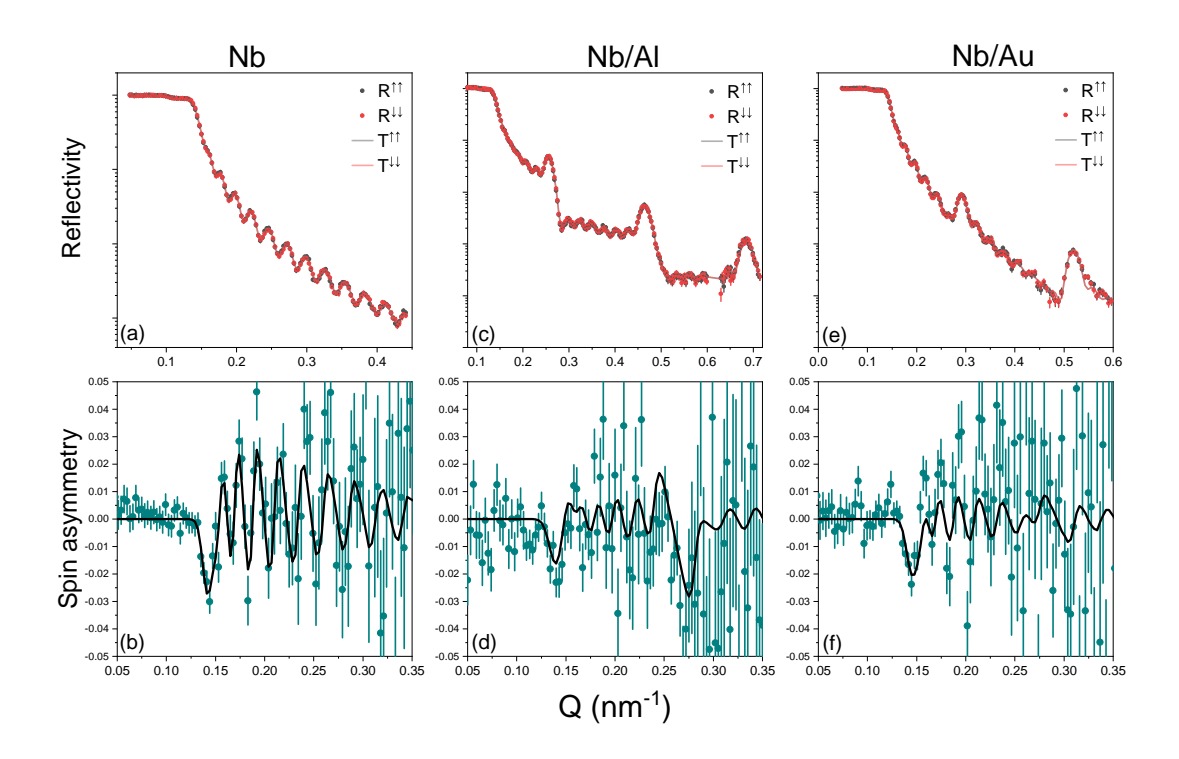


FIG. 1. Non-spin flip cross-section PNR data (points) with theoretical fits (T, line) and associated spin asymmetry for (a,b) Nb, (c,d) Nb/Al, and (e,f) Nb/Au superlattices in a field of 42 mT and temperature of 3 K. Error bars are representative of 1 σ for the data.

respectively. In this model, the external field (B_0) is fixed to the value measured with a Hall probe, while $\lambda_{\rm L}$ is a fitting parameter. Our modeling assumes that there is no flux trapped by the formation of superconducting vortices which is reasonable given that the applied field is far lower than in prior PNR reports in which vortices were not needed to explain the data [35, 37]. Furthermore, based upon our previously measured Fraunhofer patterns in Josephson junctions with a Nb/Al superconducting electrode, we found no degradation of the pattern (which is well known to occur when flux is trapped) for fields as large as 120 mT [58], which is far larger than the 40 mT applied in this work. Our fits for the 200 nm single layer of Nb yield $\lambda_{\rm L} = 96.2 \pm 9.2$ nm (uncertainties on fit parameters correspond to $2~\sigma$), which is in good agreement with prior experimental reports [34, 35, 59]. We find $\lambda_{\rm L} = 145 \pm 25$ nm and 190 ± 26 nm for the Nb/Al and Nb/Au superlattices, respectively. Our measurement of $\lambda_{\rm L}$ for the Nb/Al sample is consistent with results reported by Han et al., despite their Nb thickness being significantly thinner [37]. The increase in $\lambda_{\rm L}$ for the superlattice samples is evident from a qualitative inspection of the spin asymmetry data near Q = 0.14 nm⁻¹, as the low Q amplitude is significantly larger in Nb than the superlattices;

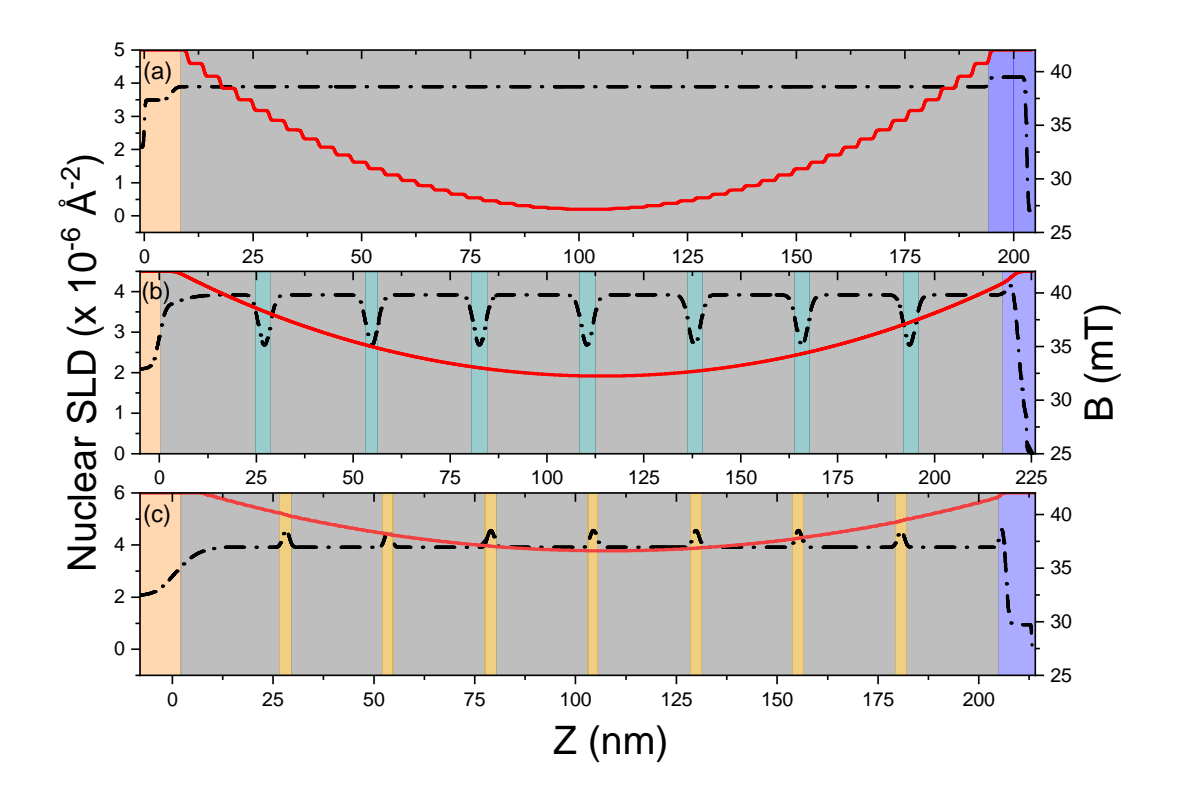


FIG. 2. Nuclear SLD (black, left axis) and magnetic field (red, right axis) for (a) 200 nm Nb, (b) Nb/Al and (c) Nb/Au superlattices as a function of depth in the sample. Z = 0 refers to the Si surface. In the Nb/Au, an additional surface layer was needed to account for condensation of gas on the sample surface that can occur at sub 10 K temperatures.

additionally the oscillations in the spin asymmetry are noticeably less clear at higher Q, in the superlattices compared to those for pure Nb.

To determine the effect of the thin Al and Au layers on the in- and out-of-plane coherence lengths, we measure H_{c2} as a function of temperature for the magnetic field applied both in- and out-of-plane, as shown in Figs. 3(a) and 3(b), respectively. Example resistance as a function of field data sets can be found in supplementary Fig. 4 [57], which is then used to determine the H_{c2} values for Fig. 3.We find that when the magnetic field is applied out-of-plane, the temperature dependence of $H_{c2\perp}$ for all samples (Fig. 3b) can be described by,

$$H_{c2} \propto (1 - T/T_{\text{critical}})$$
. (2)

When the magnetic field is applied in-plane [Fig. 3(a)], however, the superlattices and

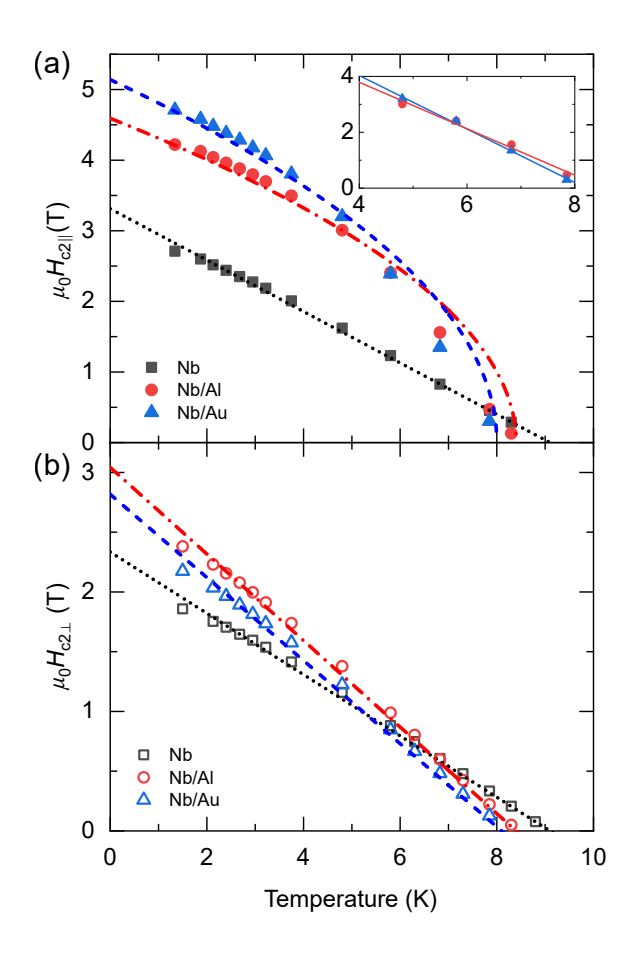


FIG. 3. Temperature dependence of H_{c2} as determined from resistance as a function of (a) in-plane and (b) out-of-plane magnetic field. The fits for Nb and out-of-plane superlattice temperature dependence are modeled using a 3D superconducting Ginzburg-Landau model, however, the in-plane superlattices are fit to the 2D model. Inset (a): A solid guide line is placed over the highest temperature data points, to highlight that under an in-plane field, the superlattices are best described linearly, as a 3D superconductor would typically behave, see text.

Nb film show very different temperature dependence. $H_{c2\parallel}$ for Nb is still best described at all temperatures by Eq. 2, which suggests the Nb film has the expected conventional 3D superconducting behavior. We also report the ratio $H_{c2\parallel}$ (0 K)/ $H_{c2\perp}$ (0 K) = 1.42. The superlattices, however, show near linear behaviour for in-plane fields close to T_{critical} , Fig. 3 (a) inset, but not at lower temperatures, causing Eq. 2 to provide unsatisfactory fits. $H_{c2\parallel}$ for the superlattices are best described overall by the 2D limit of the Ginzburg-Landau model,

$$H_{c2\parallel} \propto (1 - T/T_{\text{critical}})^{1/2},$$
 (3)

shown in Fig. 3(a). This combined with the larger ratios $H_{c2\parallel}$ (0 K)/ $H_{c2\perp}$ (0 K) = 1.52 and 1.83 for Nb/Al and Nb/Au, respectively, suggests the superlattices are 2D superconductors [48, 60].

By extracting H_{c2} from these measurements, the zero temperature ξ_{GL} can be estimated in the 3D limit from,

$$\xi_{\rm GL}(T) = \left(\frac{\Phi_0}{2\pi H_{c2}(T)}\right)^{1/2},\tag{4}$$

where Φ_0 is the flux quantum. The in-plane $\xi_{\text{GL}\parallel}(0 \text{ K})$ for Nb (determined by $H_{c2\perp}$) is estimated as $11.9 \pm 0.2 \text{ nm}$. The out-of-plane $\xi_{\text{GL}\perp}(0 \text{ K})$ for Nb (determined by $H_{c2\parallel}$) is estimated as $10.0 \pm 0.2 \text{ nm}$.

As $H_{c2\perp}$ data for the superlattices are best described as linear (3D limit), this suggests that the normal-metal layers have little influence on the in-plane screening currents, and conventional processes dominate this field orientation. Therefore, $\xi_{\text{GL}\parallel}(0 \text{ K})$ is estimated by eqn. 4 as 10.4 ± 0.3 nm for Nb/Al and 10.8 ± 0.3 nm for Nb/Au.

When the field is applied parallel to the plane of the superlattices, however, the screening currents are strongly influenced by the coupling of the Nb layers through the normal-metal layers and the impedance provided by the Nb-Al or Nb-Au interfaces. In this case it is appropriate to estimate the out-of-plane $\xi_{GL\perp}(0 \text{ K})$ in the limit of 2D layered superconductors from [48, 60],

$$\xi_{\text{GL}\perp}(T) = \left(\frac{\Phi_0}{2\pi H_{c2\perp}}\right)^{1/2} \frac{H_{c2\perp}(T)}{H_{c2\parallel}(T)}.$$
 (5)

This gives an estimate for $\xi_{\rm GL\perp}(0~{\rm K})$ for Nb/Al as $6.9\pm0.5~{\rm nm}$, and for Nb/Au (2D) as $5.9\pm0.5~{\rm nm}$.

To quantify the change of the superconducting properties when Al and Au interlayers are added, we calculate the Ginzburg-Landau parameter ($\kappa = \lambda_L/\xi_{\rm GL\perp}$). κ is found to be 8.1 \pm 0.8, 21 \pm 4, and 32 \pm 6 for the Nb, Nb/Al, and Nb/Au samples, respectively. Finally, we summarize our experimental findings for λ , ξ , H_{c2} , and κ in Table I.

Sample	$T_{ m critical}$	$\lambda_{ m L} \ (3 \ m K)$	$\mu_0 H_{c2\parallel} \ (0 \ \mathrm{K})$	$\mu_0 H_{c2\perp} \ (0 \ \mathrm{K})$	$\xi_{\mathrm{GL}\parallel}(0\ \mathrm{K})$	$\xi_{\mathrm{GL}\perp}(0~\mathrm{K})$	κ
	(K)	(nm)	(T)	(T)	(nm)	(nm)	_
Nb	9.10 ± 0.05	96.2 ± 9.2	3.29 ± 0.02	2.32 ± 0.02	$11.9 \pm 0.2 \text{ nm}$	10.0 ± 0.2	8.1 ± 0.8
Nb/Al	8.40 ± 0.05	145 ± 25	4.6 ± 0.1	3.02 ± 0.03	$10.4 \pm 0.3 \text{ nm}$	6.9 ± 0.5	21 ± 4
Nb/Au	8.00 ± 0.05	190 ± 26	5.1 ± 0.1	2.81 ± 0.04	$10.8 \pm 0.3 \text{ nm}$	5.9 ± 0.5	32 ± 6

TABLE I. Summary of experimentally measured superconducting parameters for Nb, Nb/Al and Nb/Au samples. $\xi_{\text{GL}\parallel}$ and $\xi_{\text{GL}\perp}$ are determined for Nb from the 3D limit, and for the superlattices from the layered 2D superconductor limit of the Ginzburg-Landau formulation.

IV. DISCUSSION

From the combination of PNR, XRR, and electrical transport, we develop a consistent picture of the means by which the superconducting properties are affected by the structural differences between the S/N superlattices and uniform superconducting films of similar thickness. The fits for the PNR and XRR show that the repeated layers in our superlattices are uniform with near nominal deposition thicknesses and SLD values close to bulk. The XRR fitted roughnesses of the topmost surface for the Nb/Al and Nb/Au superlattices (0.60 and 0.69 nm, respectively) are smaller than those obtained for the Nb film (1.95 nm). The improved surface roughness of the superlattices is qualitatively consistent with trends reported for similar Nb and Nb/Al samples with root-mean-squared roughnesses of 0.53 and 0.23 nm, respectively, obtained from atomic force microscopy over an area of 1 μ m⁻² [31]. Note that the roughness values obtained from reflectivity measurements are typically larger than those obtained from atomic force microscopy since they represent an average of interdiffusion, local roughness, and large-scale features averaged across the sample plane. We also note that the Nb/Al sample characterized by Wang et al. had a superlattice repeat of 3 [31], and not 7 as we use in this work. We also observe satellite (Yoneda) peaks in the rocking curve for the Nb film at θ positions of θ_C (where θ_C corresponds to the critical angle for total internal reflection in Nb) and 2θ - θ_C . Youeda peaks, however, are not apparent in comparable rocking curves for the Nb/Al and Nb/Au samples. In general, Yoneda scattering results from a resonant enhancement of scattering from faceted surfaces. Since these features can be qualitatively linked to surface roughness, the pronounced Yoneda wings in rocking curves for the Nb film suggest that its surface is significantly rougher than the surfaces of the superlattices [61] (see supplementary Fig. 2 [57]).

Prior studies demonstrated that the thin intermediary layers (Al and Au in this work) disrupt the columnar growth of Nb, resulting in reduced surface roughness in Nb/N superlattices [28, 30]. This conclusion is further supported by XRR measurements of the off-specular background for the superlattices and film. While the off-specular scattering for the Nb film is mostly featureless (supplemental Fig. 1c [57]), the scattering for the superlattices has finite-size oscillations (with constant spacing in Q) and diffraction peaks that mirror the features present in the specular reflectivity (supplemental Fig. 1 [57]). The presence of these off-specular oscillations suggests that the in-plane interface roughness originates in the layers near the substrate and is replicated from one layer to the next (i.e., conformal) [61–63]. The superlattice interfaces are presumably well-defined on a local scale, and the resulting smooth surface contrasts with that of the Nb film.

To maintain the best possible superconducting properties for the superlattice, it is important that the structural characteristics of the superlattice ensure that N layers are well proximitized by the superconductor. The proximity effect in Nb/Al has been studied extensively [37, 46, 64]. In Nb/Al bilayers, the Al will superconduct via the proximity effect and form a fully opened superconducting gap for thin Al layers and transparent interfaces such as those discussed by Golubov *et al* [64]. We estimate the normal metal coherence length for Al at 3 K, associated with the proximity effect, in the diffusive limit to be $\xi_N = 65$ nm [65, 66]. Nb/Au is less well studied, however measurements suggest that Au can support superconducting correlations over several tens of nanometers [39], which is consistent with the estimated $\xi_N = 85$ nm in the diffusive limit at 3 K [65, 66].

Despite the expected strong proximity effect in the Al and Au layers, the temperature dependence of $H_{c2\parallel}$ for the superlattices is best described by the 2D limit, except near T_{critical} where ξ_S diverges (see Fig 3(a) inset). This suggests decoupling of the individual Nb layers by the Al or Au spacers. The decoupling of the Nb layers is consistent with the reduced T_{critical} of the superlattices. Similar behaviour in $H_{c2}(T)$ has been widely studied in layered S/N superlattices in the context of 3D to 2D superconductivity crossover [47], which is predicted to occur when the N layer thickness is on order of ξ_{\perp} [60]. In Nb/Cu multilayers, the crossover is reported for a Cu thickness of 33.3 nm, consistent with the prediction [48]. What is unusual in our case is that the N layers under study (2.4 nm) are much thinner than theory would predict for the 3D/2D crossover to occur. Another

feasible explanation is that the S/N interface transparency (γ_B in Golubov et al [64]) is poor enough that there is a significant reflection probability at the interface, and so this lack of transparency decouples the S layers. However, Houwman et al. measured the role of the interface in Nb/Al on proximity superconductivity, and determined that the potential barrier at the Nb/Al interface is negligible ($\gamma_B < 0.05$) [67]. Thus, it is surprising that the H_{c2} (T) of our superlattices is best described by the 2D limit for layered superconductors, since 2D decoupling in multilayers or interface transparency of proximity superconductivity are not sufficient to account for this behavior.

Experimental measurements of the penetration depth ($\lambda_{\rm L}^{\rm experimental}$) are known to be larger than the intrinsic London penetration depth ($\lambda_{\rm L}^{\rm intrinsic}$), due to impurity defects. A relationship between the intrinsic London penetration depth and that measured by experiment has been derived by Pippard [68] and demonstrated by Zhang *et al* [35], as

$$\lambda_{\rm L}^{\rm experimental} = \lambda_{\rm L}^{\rm intrinsic} \sqrt{1 + \frac{\xi_{\rm GL}}{l}},$$
 (6)

where l is the electron's mean free path (10.4 nm [35]), and valid when $l \ll \lambda$. Using the experimental values for $\lambda_{\rm L}$ and $\xi_{\rm GL}$ for Nb, we calculate $\lambda_{\rm L}^{\rm intrinsic} = 62$ nm. Other groups have reported a value for $\lambda_{\rm L}^{\rm intrinsic}$ in Nb thin films on order of 43 nm, however, these publications rely on utilizing the clean limit of $\xi_{\rm GL}$ for Nb (as reported by Weber *et al* [69] and taken to be 41 nm by Zhang *et al* [35]), whereas we utilize our measured value of $\xi_{\rm GL}$.

Finally, our measured penetration depth for Nb/Al is in agreement with prior reports by Han et al [37] using PNR and Madden et al [15], who could simulate the inductance of their SQUIDs only if they used a longer $\lambda_{\rm L}$ (185 nm) for Nb/Al (with 3 multilayer repeats) than was expected from pure Nb.

V. CONCLUSIONS

In summary, we have studied the effect of adding a thin normal-metal layer between Nb layers by directly measuring the London penetration depth and Ginzburg-Landau coherence length. We report an experimentally determined Ginzburg-Landau parameter for Nb, $\kappa = \lambda_{\rm L}/\xi_{\rm GL} = 8.1 \pm 0.8$, and for the superlattices Nb/Al, $\kappa = 21 \pm 4$ and Nb/Au, $\kappa = 32 \pm 6$. These differences in κ are driven by the superlattices having a significantly longer penetration depth and shorter coherence length compared to Nb films of similar thickness. The changes

suggest that the addition of a thin N layer between the S layers increases the disorder in the superconducting system despite the expectation that the N layer would be fully proximitized given that the coherence length is large with respect to the N layer thickness. Furthermore, we find that the superlattices act as a layered 2D superconductor, unlike the Nb sample that has 3D behavior. The lower surface roughness associated with using a S/N superlattice compared to a single S layer is valuable in Josephson junction applications given the overall improved quality of the junction, however, this has the unintended consequence of changing characteristic superconducting properties. To properly model such systems, one must account for changes in $\lambda_{\rm L}$, $\xi_{\rm GL}$, and $T_{\rm critical}$ —which we independently and directly measure in this work.

The data associated with this paper are openly available from the NCNR and University of Leeds data repositories [70].

ACKNOWLEDGMENTS

We thank Alexander Grutter and Yury Khaydukov for helpful discussions, Josh Willard for initial characterization of the superlattices, and Tanya Dax, Joseph Dura and Brian Maranville for assistance with the PNR measurements. P.Q. acknowledges support from the National Research Council Research Associateship Program. This project has received funding from the European Unions Horizon 2020 research and innovation programme under the Marie Skłodowska-Curie Grant Agreement No. 743791 (SUPERSPIN).

P. Quarterman and N. Satchell contributed equally to this work.

^[1] H. Kamerlingh-Onnes, Leiden Comm. **120b**, **122b**, **124c** (1911).

^[2] W. Meissner and R. Ochsenfeld, Naturwissenschaften 21, 787 (1933).

^[3] C. Kittel, Introduction to Solid State Physics, Vol. 8 (Wiley New York, 1976).

^[4] D. S. Holmes, A. L. Ripple, and M. A. Manheimer, IEEE Trans. Appl. Supercond 23, 1701610 (2013).

^[5] I. I. Soloviev, N. V. Klenov, S. V. Bakurskiy, M. Y. Kupriyanov, A. L. Gudkov, and A. S. Sidorenko, Beilstein J. Nanotechnol 8, 2689 (2017).

- [6] C. Bell, G. Burnell, C. W. Leung, E. J. Tarte, D.-J. Kang, and M. G. Blamire, Appl. Phys. Lett. 84, 1153 (2004).
- [7] C. Bell, G. Burnell, C.W. Leung, E. J. Tarte, and M. G. Blamire, IEEE Trans. Appl. Supercond 15, 908 (2005).
- [8] B. Baek, W. H. Rippard, S. P. Benz, S. E. Russek, and P. D. Dresselhaus, Nat. Commun. 5, 3888 (2014).
- [9] M. Abd El Qader, R. K. Singh, S. N. Galvin, L. Yu, J. M. Rowell, and N. Newman, Appl. Phys. Lett. 104, 022602 (2014).
- [10] B. Baek, W. H. Rippard, M. R. Pufall, S. P. Benz, S. E. Russek, H. Rogalla, and P. D. Dresselhaus, Phys. Rev. Appl. 3, 011001 (2015).
- [11] E. C. Gingrich, B. M. Niedzielski, J. A. Glick, Y. Wang, D. L. Miller, R. Loloee, W. P. Pratt, and N. O. Birge, Nat. Phys. 12, 564 (2016).
- [12] I. Dayton, T. Sage, E. Gingrich, M. Loving, T. Ambrose, N. Siwak, S. Keebaugh, C. Kirby, D. Miller, A. Herr, Q. Herr, and O. Naaman, IEEE Magn. Lett. 9, 3301905 (2018).
- [13] B. M. Niedzielski, T. J. Bertus, J. A. Glick, R. Loloee, W. P. Pratt, and N. O. Birge, Phys. Rev. B 97, 024517 (2018).
- [14] J. A. Glick, V. Aguilar, A. B. Gougam, B. M. Niedzielski, E. C. Gingrich, R. Loloee, W. P. Pratt, and N. O. Birge, Sci. Adv. 4, eaat9457 (2018).
- [15] A. E. Madden, J. C. Willard, R. Loloee, and N. O. Birge, Supercond. Sci. Technol 32, 015001 (2018).
- [16] N. O. Birge, A. E. Madden, and O. Naaman, Proc. SPIE 10732, 107321M (2018).
- [17] N. O. Birge and M. Houzet, IEEE Magn. Lett. 10, 4509605 (2019).
- [18] N. Satchell, P. M. Shepley, M. Algarni, M. Vaughan, E. Darwin, M. Ali, M. C. Rosamond, L. Chen, E. H. Linfield, B. J. Hickey, and G. Burnell, Appl. Phys. Lett. 116, 022601 (2020).
- [19] F. S. Bergeret, A. F. Volkov, and K. B. Efetov, Phys. Rev. Lett. 86, 4096 (2001).
- [20] R. Keizer, S. Goennenwein, T. Klapwijk, G. Miao, G. Xiao, and A. Gupta, Nature 439, 825 (2006).
- [21] T. S. Khaire, M. A. Khasawneh, W. P. Pratt, and N. O. Birge, Phys. Rev. Lett. 104, 137002 (2010).
- [22] J. W. A. Robinson, J. D. S. Witt, and M. G. Blamire, Science **329**, 59 (2010).
- [23] M. S. Anwar, F. Czeschka, M. Hesselberth, M. Porcu, and J. Aarts, Phys. Rev. B 82, 100501

- (2010).
- [24] W. M. Martinez, W. P. Pratt, and N. O. Birge, Phys. Rev. Lett. 116, 077001 (2016).
- [25] K. Lahabi, M. Amundsen, J. A. Ouassou, E. Beukers, M. Pleijster, J. Linder, P. Alkemade, and J. Aarts, Nat. Commun. 8, 2056 (2017).
- [26] N. O. Birge, Philos. Trans. Royal Soc. A 376, 20150150 (2018).
- [27] R. K. Singh, N. D. Rizzo, M. Bertram, K. Zheng, and N. Newman, IEEE Magn. Lett. 9, 5100904 (2018).
- [28] J. Chen, E. D. Rippert, S. N. Song, M. P. Ulmer, and J. B. Ketterson, J. Mater. Res. 9, 1678 (1994).
- [29] H. Kohlstedt, F. König, P. Henne, N. Thyssen, and P. Caputo, J. Appl. Phys. 80, 5512 (1996).
- [30] C. D. Thomas, M. P. Ulmer, and J. B. Ketterson, J. Appl. Phys. 84, 364 (1998).
- [31] Y. Wang, W. P. Pratt, and N. O. Birge, Phys. Rev. B. 85, 214522 (2012).
- [32] S. J. Blundell, Contemp. Phys. 40, 175 (1999).
- [33] S. M. Anlage, V. V. Talanov, and A. R. Schwartz, "Principles of near-field microwave microscopy," in Scanning Probe Microscopy: Electrical and Electromechanical Phenomena at the Nanoscale, edited by S. Kalinin and A. Gruverman (Springer New York, New York, NY, 2007) pp. 215–253.
- [34] G. P. Felcher, R. T. Kampwirth, K. E. Gray, and R. Felici, Phys. Rev. Lett. 52, 1539 (1984).
- [35] H. Zhang, J. W. Lynn, C. F. Majkrzak, S. K. Satija, J. H. Kang, and X. D. Wu, Phys. Rev. B 52, 10395 (1995).
- [36] A. J. Drew, M. W. Wisemayer, D. O. G. Heron, S. Lister, S. L. Lee, A. Potenza, C. H. Marrows, R. M. Dalgliesh, T. R. Charlton, and S. Langridge, Phys. Rev. B 80, 134510 (2009).
- [37] S. W. Han, J. Farmer, P. F. Miceli, G. Felcher, R. Goyette, G. T. Kiehne, and J. B. Ketterson, Physica B 336, 162 (2003).
- [38] A. Di Bernardo, Z. Salman, X. L. Wang, M. Amado, M. Egilmez, M. G. Flokstra, A. Suter, S. L. Lee, J. H. Zhao, T. Prokscha, E. Morenzoni, M. G. Blamire, J. Linder, and J. W. A. Robinson, Phys. Rev. X 5, 041021 (2015).
- [39] M. G. Flokstra, N. Satchell, J. Kim, G. Burnell, P. J. Curran, S. J. Bending, J. F. K. Cooper, C. J. Kinane, S. Langridge, A. Isidori, N. Pugach, M. Eschrig, H. Luetkens, A. Suter, T. Prokscha, and S. L. Lee, Nat. Phys. 12, 57 (2016).
- [40] M. G. Flokstra, R. Steward, N. Satchell, G. Burnell, H. Luetkens, T. Prokscha, A. Suter,

- E. Morenzoni, S. Langridge, and S. L. Lee, Phys. Rev. Lett. 120, 247001 (2018).
- [41] Y. N. Khaydukov, E. A. Kravtsov, V. D. Zhaketov, V. V. Progliado, G. Kim, Y. V. Nikitenko, T. Keller, V. V. Ustinov, V. L. Aksenov, and B. Keimer, Phys. Rev. B. 99, 140503(R) (2019).
- [42] R. Stewart, M. G. Flokstra, M. Rogers, N. Satchell, G. Burnell, D. Miller, H. Luetkens, T. Prokscha, A. Suter, E. Morenzoni, and S. L. Lee, Phys. Rev. B 100, 020505 (2019).
- [43] M. G. Flokstra, R. Stewart, N. Satchell, G. Burnell, H. Luetkens, T. Prokscha, A. Suter, E. Morenzoni, S. Langridge, and S. L. Lee, Appl. Phys. Lett 115, 072602 (2019).
- [44] S. Mironov, A. S. Mel'nikov, and A. Buzdin, Appl. Phys. Lett. 113, 022601 (2018).
- [45] M. Tinkham, Introduction to Superconductivity: Second Edition (Dover Books on Physics), 2nd ed. (Dover Publications, 2004).
- [46] A. Barone and G. Paternò, *Physics and Applications of the Josephson Effect* (John Wiley & Sons, New York, 1982).
- [47] B. Y. Jin and J. B. Ketterson, Adv. Phys 38, 189 (1989).
- [48] C. S. L. Chun, G.-G. Zheng, J. L. Vincent, and I. K. Schuller, Phys. Rev. B. 29, 4915 (1984).
- [49] K. Kanoda, H. Mazaki, T. Yamada, N. Hosoito, and T. Shinjo, Phys. Rev. B 33, 2052 (1986).
- [50] S. T. Ruggiero, T. W. Barbee, and M. R. Beasley, Phys. Rev. Lett. 45, 1299 (1980).
- [51] D. Neerinck, K. Temst, C. Van Haesendonck, Y. Bruynseraede, A. Gilabert, and I. K. Schuller, Phys. Rev. B 43, 8676 (1991).
- [52] F. Y. Ogrin, S. L. Lee, A. D. Hillier, A. Mitchell, and T. H. Shen, Phys. Rev. B. 62, 6021 (2000).
- [53] B. Maranville, W. Ratcliff II, and P. Kienzle, Journal of Applied Crystallography 51, 1500 (2018).
- [54] B. J. Kirby, P. A. Kienzle, B. B. Maranville, N. F. Berk, J. Krycka, F. Heinrich, and C. F. Majkrzak, Curr. Opin. Colloid Interface Sci. 17, 44 (2012).
- [55] P. Kienzle, B. B. Maranville, and B. Kirby, "Reflectometry software," https://www.nist.gov/ncnr/data-reduction-analysis/reflectometry-software.
- [56] International Organization for Standardization, Guide to the Expression of Uncertainty in Measurement (JCGM, 2008).
- [57] See Supplemental Material at [URL will be inserted by publisher] for x-ray characterization, additional PNR data above T_{critical} , additional transport data, and details for calculations and analysis reported in the text.

- [58] J. A. Glick, S. Edwards, D. Korucu, V. Aguilar, B. M. Niedzielski, R. Loloee, W. P. Pratt, N. O. Birge, P. G. Kotula, and N. Missert, Phys. Rev. B 96, 224515 (2017).
- [59] Y. Khaydukov, R. Morari, L. Mustafa, J. H. Kim, T. Keller, S. Belevski, A. Csik, L. Tagirov, G. Logvenov, A. Sidorenko, and B. Keimer, J. Supercond. Nov. Magn. 28, 1143 (2015).
- [60] R. A. Klemm, A. Luther, and M. R. Beasley, Phys. Rev. B 12, 877 (1975).
- [61] S. K. Sinha, E. B. Sirota, S. Garoff, and H. B. Stanley, Phys. Rev. B 38, 2297 (1988).
- [62] J. M. Freitag and B. M. Clemens, J. Appl. Phys. 89, 1101 (2001).
- [63] H. Zabel, Appl. Phys. A. 58, 159 (1994).
- [64] A. A. Golubov, E. P. Houwman, J. G. Gijsbertsen, J. Flokstra, H. Rogalla, J. B. le Grand, and P. A. J. de Korte, Phys. Rev. B 49, 12953 (1994).
- [65] A. I. Buzdin, Rev. Mod. Phys. 77, 935 (2005).
- [66] D. Gall, J. Appl. Phys **119**, 085101 (2016).
- [67] A. A. Golubov, E. P. Houwman, J. G. Gijsbertsen, V. M. Krasnov, J. Flokstra, H. Rogalla, and M. Y. Kupriyanov, Phys. Rev. B 51, 1073 (1995).
- [68] A. B. Pippard, Proc. R. Soc. Lond. A **216**, 547 (1953).
- [69] H. W. Weber, E. Seidl, C. Laa, E. Schachinger, M. Prohammer, A. Junod, and D. Eckert, Phys. Rev. B 44, 7585 (1991).
- [70] P. Quarterman, and N. Satchell, Distortions to the penetration depth and coherence length of superconductor/normal-metal superlattices - dataset. University of Leeds, 2020, https://doi.org/10.5518/767.

Supplementary Material for "Distortions to the penetration depth and coherence length of superconductor/normal-metal superlattices" by P. Quarterman et al.

X-ray reflectivity is collected on the samples uing a Cu-K α source (supplementary Fig. 1(a)), and the resulting fits to the data yield scattering length density profiles, shown in supplementary Fig. 1(b), in strong agreement with the polarized neutron reflectometry results. Off-specular scattering is collected to use for background subtraction by offsetting θ and scanning θ -2 θ in order to sample the Q_z dependence of the in-plane disorder (Fig. 1(c)). For the off-specular background scattering in the Nb sample, we observe no Q-dependent oscillations, as expected. However, in the superlattices the background scans show strong periodic oscillations. These off-specular oscillations have been shown to be indicative of conformal roughness [1,2].

Rocking curves are shown for the Nb, Nb/Al, and Nb/Au samples in Fig. 2. The Nb rocking curve at $2\theta = 1.2^{\circ}$ shows pronounced peaks (Yoneda wings) near $\theta \approx \theta_C$ and $2\theta - \theta_C$, where θ_C is the critical angle. These Yoneda peaks are suggestive of significant surface roughness [3]. In contrast, the only pronounced peaks observed in the Nb/Al and Nb/Au rocking curves are the specular reflections, which are on top of broad diffuse scattering for the latter sample. In the Nb/Au rocking curve at $2\theta = 1.3^{\circ}$, there are peak-like artifacts symmetric about the specular reflection. In the rocking curve measured at $2\theta = 2.2^{\circ}$, however, these features do not shift outward in a manner consistent with Yoneda scattering. In qualitative comparison to those of the Nb film, the surfaces of the Nb/N superlattices appear to be relatively smooth on a local scale.

The spin asymmetry for the Nb/Al superlattice taken at 20 K is shown in supplemental Fig. 3, and as expected we see no observable magnetic contribution to the PNR. Similar observations are seen for the Nb and Nb/Au samples taken when measured above the superconducting critical temperature of the samples.

We determine the upper critical fields $(H_{c2\parallel})$ and $H_{c2\perp}$ by measuring resistance as a function of field (R vs. H); typical R vs. H curves for the field applied in-plane and out-of-plane are shown in supplemental Fig. 4. H_{c2} is determined by taking the peak of the first derivative of the resistance with respect to field, and averaging the result obtained at the positive and negative field regime.

In the main text, we estimate the normal state coherence length (ξ_N) in the diffusive (dirty) limit for Al and Au following Buzdin [4],

$$\xi_N = \sqrt{\frac{\hbar D}{2\pi k_B T}},\tag{1}$$

where D is the diffusion coefficient, $D = \frac{1}{3}v_{\rm F}l$, and $v_{\rm F}$ and l are the Fermi velocity and mean free path respectively. Values for $v_{\rm F}$ and l are taken from Gall [5], with the limitation that l is calculated by Gall at room temperature.

- [1] H. Zabel, Appl. Phys. A. 58, 159 (1994).
- [2] J. M. Freitag and B. M. Clemens, J. Appl. Phys. 89, 1101 (2001).
- [3] D. E. Savage, J. Kleiner, N. Schimke, Y. Phang, T. Jankowski, J. Jacobs, R. Kariotis, and M. G. Lagally, J. Appl. Phys 69, 1411 (1991).
- [4] A. I. Buzdin, Rev. Mod. Phys. 77, 935 (2005).
- [5] D. Gall, J. Appl. Phys **119**, 085101 (2016).

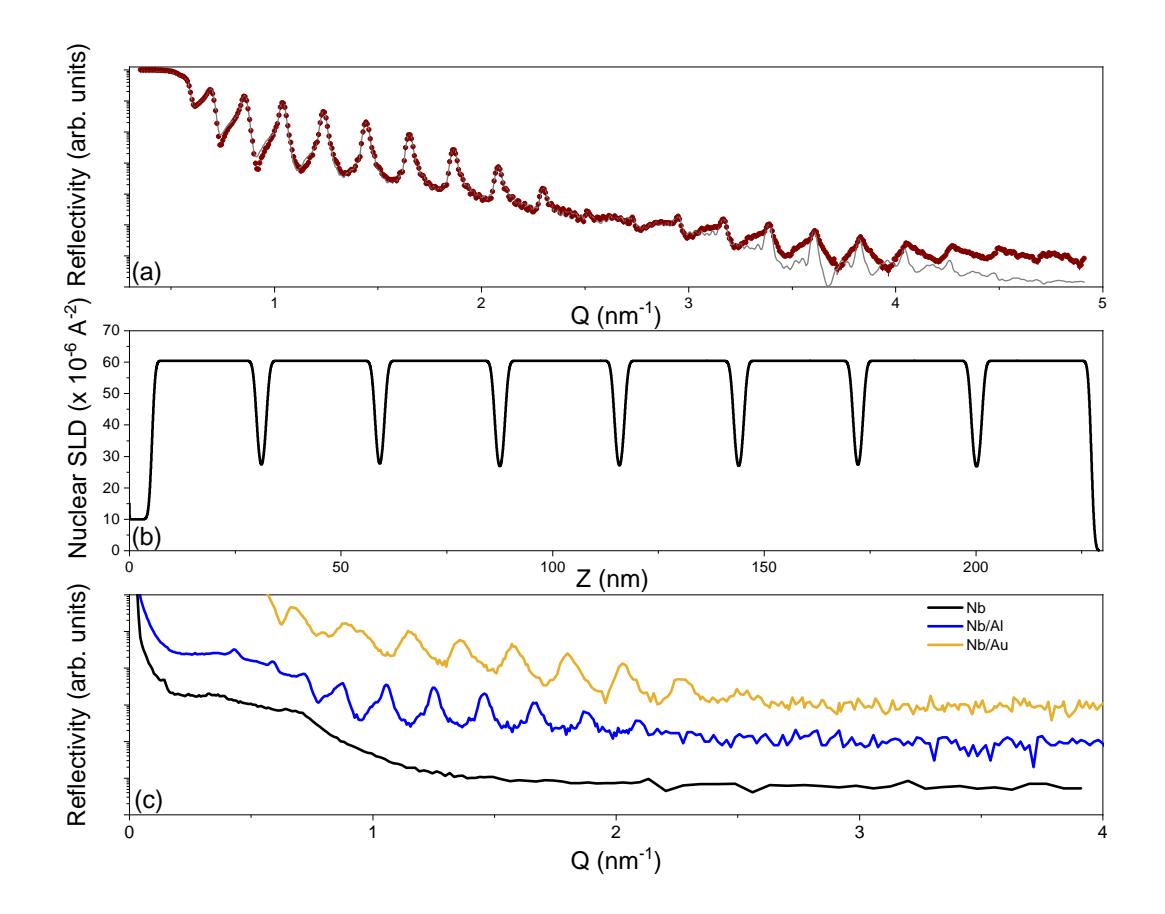


FIG. 1. (a) XRR data and model for Nb/Al, with a corresponding SLD profile shown in (b). (c) Off-specular x-ray reflectivity for the Nb, Nb/Al and Nb/Au samples. The superlattices show pronounced oscillations in the off-specular signal, which are indicative of conformal roughness.

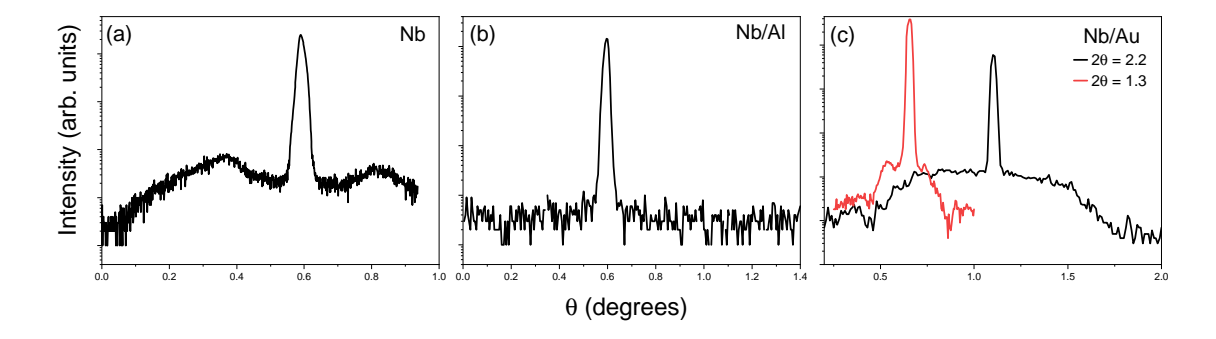


FIG. 2. X-ray rocking curves of (a) Nb, (b) Nb/Al, and (c) Nb/Au samples. The Nb and Nb/Al rocking curves were obtained at $2\theta = 1.2^{\circ}$. Rocking curves for Nb/Au were measured at $2\theta = 1.3^{\circ}$ for direct comparison to (a) and (b) and at $2\theta = 2.2^{\circ}$ at the maximum of a specular superlattice peak. A comparison of these two curves suggests that the apparent features in the diffuse scattering are not consistent with Yoneda scattering.

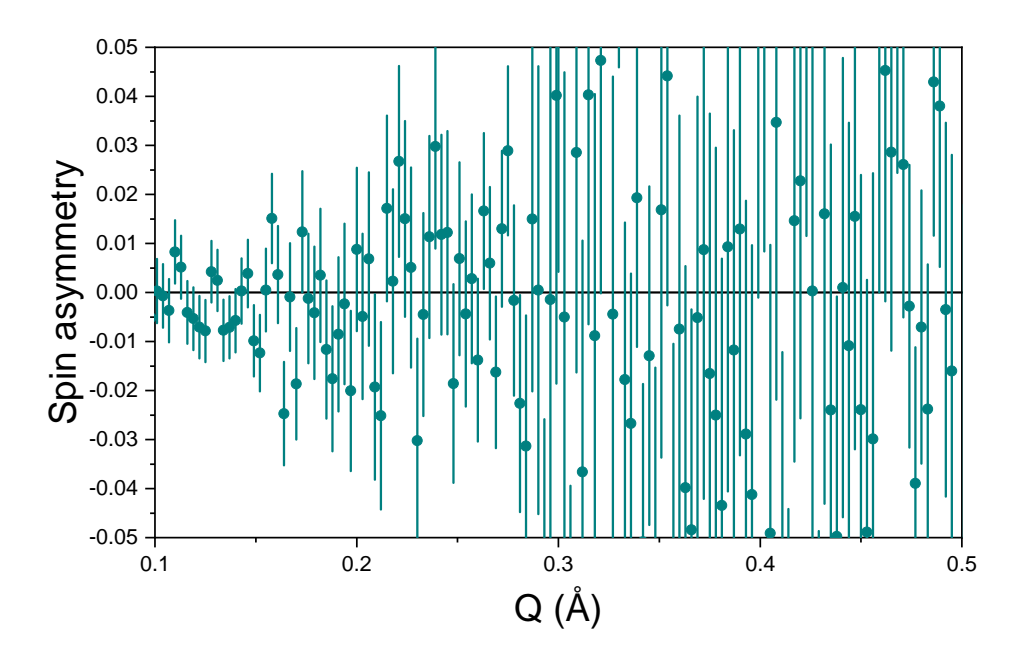


FIG. 3. Spin asymmetry for Nb/Al superlattice collected at 20 K, which is above the superconducting critical temperature of the sample. Error bars are representative of 1σ

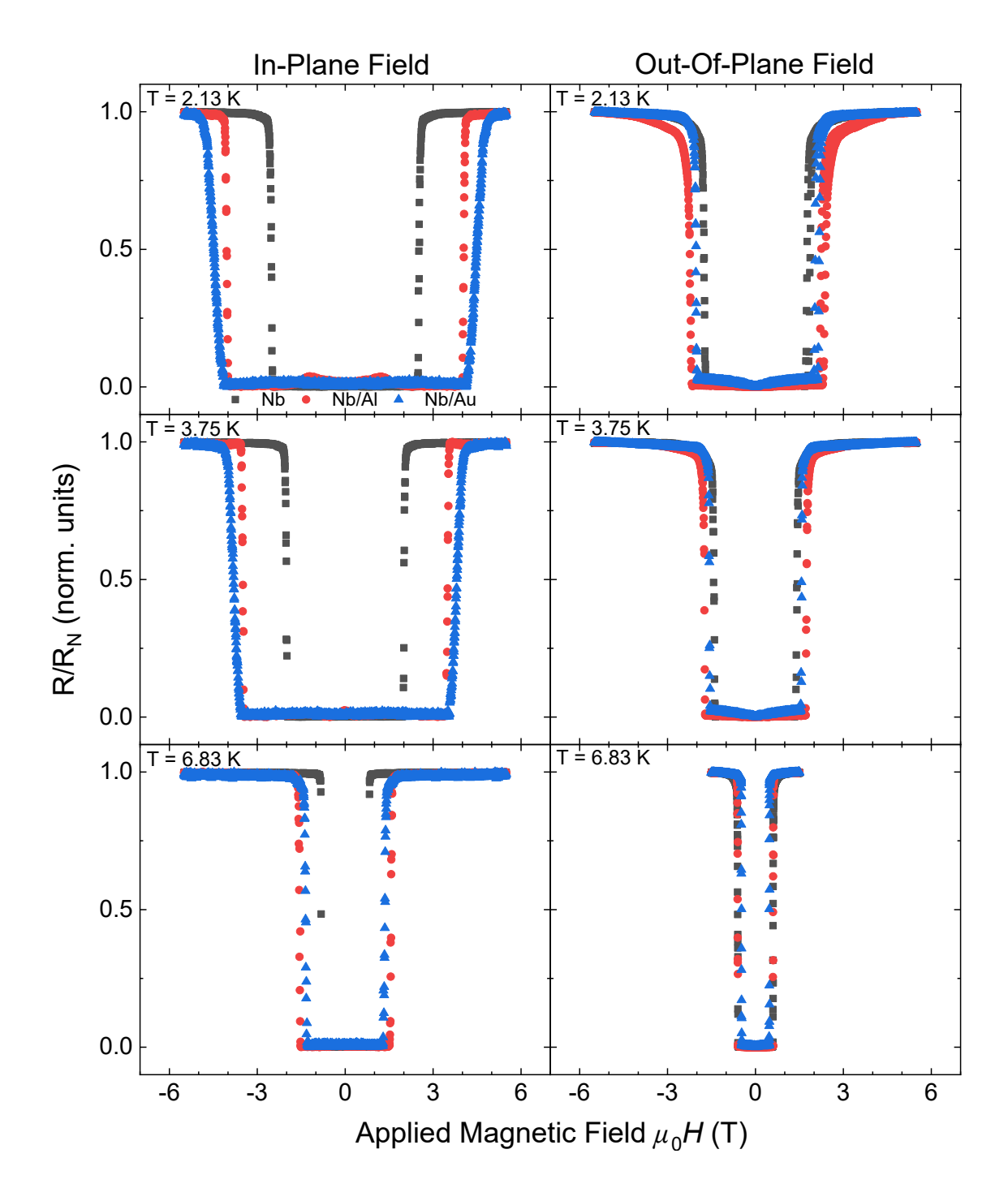


FIG. 4. Resistance vs magnetic field for the Nb (black, squares), Nb/Al (red, circles), and Nb/Au (blue, triangles) samples to determine $H_{c2\parallel}$ and $H_{c2\perp}$.